Journal of Engineering Physics and Thermophysics, Vol. 76, No. 5, 2003

INFLUENCE OF MULTIPLE-SCATTERING PROCESSES ON THE LASER PROBING OF BIOLOGICAL TISSUES

N. B. Bazylev, E. I. Lavinskaya, and N. A. Fomin

UDC 53:082.53+535.36

Theoretical aspects of multiple-scattering processes in laser probing of biological tissues have been considered. The method of digital dynamic speckle-photography has been described. The results of experimental studies of the near-surface blood flow and stressed-strained states in a pin-structure–tooth-root model are presented.

Introduction. New biomedical applications of lasers are an extremely important and rapidly developing interdisciplinary direction at the juncture of laser physics, optics of scattering media, biophysics, and engineering physics, including the current methods of diagnostics and control based on deep computer real- or quasi-real-time processing of measurement data. The laser probing of biological tissues has a 40-year history and is already a separate direction. Its rapid development in the last two decades was stimulated by the advances in laser engineering and digital technologies of entering images into a PC (personal computer) with the use of CCD-cameras (CCD — charge-coupled device) in combination with the experience of accumulation of huge bodies of experimental information and its statistical analysis [1–4]. As in diagnosing technical flows, in investigating biological tissues and organs, the most successful techniques proved to be the application of laser speckle-fields consisting of micron "granules" of radiation that are virtual reference points in the cross-correlation analysis of obtained images of investigated biological tissues. In thermal physics and in the physics of fast processes, such methods of investigation are called digital dynamic speckle-photography (DDSP) and digital dynamic speckle-interferometry (DDSI) [5]. (In recording dynamic changes, these methods rather pertain to cinematography, and, more exactly, to cinematography of fast processes. For one- or two-exposure recording, these methods are referred to as DSI and DSP, respectively). While the DSI (digital speckle-interferometry) schemes are traditionally used in physical experiments, the DSP (digital speckle-photography) has come into use relatively recently [6]. This is due to the fact that the recording of initial speckle-fields requires a higher spatial resolution than the recording of interference fringes arising under the interference of these speckle-fields in the DSI. In terms of mathematics, the DSP uses the same techniques of space-time cross-correlation analysis as those used in the popular Digital Particle Image Velocimetry (DPIV) methods of digital measurement of particle velocities, which are a development of the "photographic" Particle Image Velocimetry (PIV) systems of particle velocity measurement [7]. Analogs of speckle-fields in PIV and DPIV are "snapshot" photographs visualizing the flow of microscopic particles moving together with the mainstream flow and localized in a certain flow plane by means of a so-called laser knife. The present work is devoted to the development of DDSP methods as applied to the diagnostics of biological tissues, one of whose basic features is the formation of biospeckle-fields with the participation of the processes of multiple scattering of the probing radiation.

Formation of Biospeckle-Fields and Their Dynamics. As a result of the coherent radiation scattering in a diffuse object and the three-dimensional interference of the scattered radiation, a so-called speckle-field consisting of tiny granules of radiation — speckles having characteristic sizes of the order of 1–2 μm — is created. Analogous speckle-fields are also created under laser radiation scattering by biological tissues. For instance, the visible light penetrating into the human skin to a depth of 1–2 mm is scattered by the erythrocytes of blood flowing in tiny tissue capillaries. As a result of the multiple-scattering processes, a dynamic biospeckle-field varying in space and time as a result of the erythrocyte motion is formed. Thus, the biological tissue image obtained in coherent light differs from the normal photograph by the presence of an additional biospeckle-field, which is a spurious noise for normal photography

A. V. Luikov Heat and Mass Transfer Institute, National Academy of Sciences of Belarus, 15 P. Brovka Str., Minsk, 220072, Belarus; email: fomin@hmti.ac.by. Translated from Inzhenerno-Fizicheskii Zhurnal, Vol. 76, No. 5, pp. 16–24, September–October, 2003. Original article submitted March 4, 2003.

1062-0125/03/7605-0969$25.00

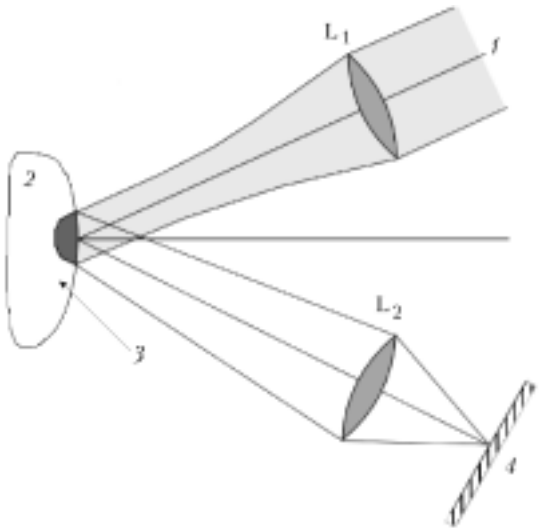

Fig. 1. Biospeckle-field formation upon laser probing of the biological tissue: 1) Gaussian beam; 2) biological tissue *in vivo*; 3) illuminated volume; 4) observation plane (L_1, L_2 — lenses).

and at the same time a carrier of the richest information in modern DDSP and DDSI schemes. One can get an impression about the volume of such information, taking into account that each square millimeter of the speckle-field contains about a million elementary radiation granules — speckles varying in time with the frequencies characteristic of the medium being investigated. For biological tissues, these frequencies are from 1 Hz to a few kilohertz, providing information flows of a few gigabits per second (10^9 bits) from each square millimeter of the tissue under investigation.

The dynamic properties of the classical speckle-fields formed by moving rough objects have been investigated in fair detail (see, e.g., [8]). However, the biospeckle-fields arising from multiple-scattering processes have received much less study. The most general way of describing the space-time variations of speckle-fields is by using space-time correlation formulas. In the normalized form for the fluctuating component $\Delta I = I - \langle I \rangle$ of the radiation intensity in the speckle-field this function can be given by the coefficient $\gamma_{\Delta I}$:

$$\gamma_{\Delta I}(\mathbf{r}_1, \mathbf{r}_2; t_1, t_2) = \frac{\langle \Delta I(\mathbf{r}_1, t_1) \cdot \Delta I(\mathbf{r}_2, t_2) \rangle}{\langle \Delta I(\mathbf{r}_1, t_1) \cdot \Delta I(\mathbf{r}_2, t_2) \rangle}. \quad (1)$$

This quantity characterizes the mutual correlation of two speckle-fields obtained at different points in space and at different instants of time and varies from 0 to 1.

Two basic methods of changing speckle-fields are distinguished: "displacement" of speckle-fields, when a certain set of speckles is displaced as a unity without changing their relative position and "boiling" of speckles, when separate speckles chaotically appear and disappear at the same points in space, experiencing no noticeable displacements.

Function (1) depends on many factors. One of the most important of them is the form of the laser beam forming the speckle-field. For the Gaussian form of the beam, when it is focused on the surface near the biological tissue, the spot diameter ω and the wavefront curvature ρ are expressed as functions of the distance z from the position of the beam waist (1):

$$\omega = \omega_0 \left[1 + \left(\frac{z}{z_0} \right)^2 \right]^{1/2}, \quad \rho = z \left[1 + \left(\frac{z}{z_0} \right)^2 \right]^{1/2}. \quad (2)$$

Here $z_0 = \pi\omega_0^2/\lambda$. Two parameters — the correlation time τ_c and the delay time τ_d — were introduced in (8) to describe the dynamic properties of speckle-fields simultaneously experiencing two modes of change — "displacement" and "boiling":

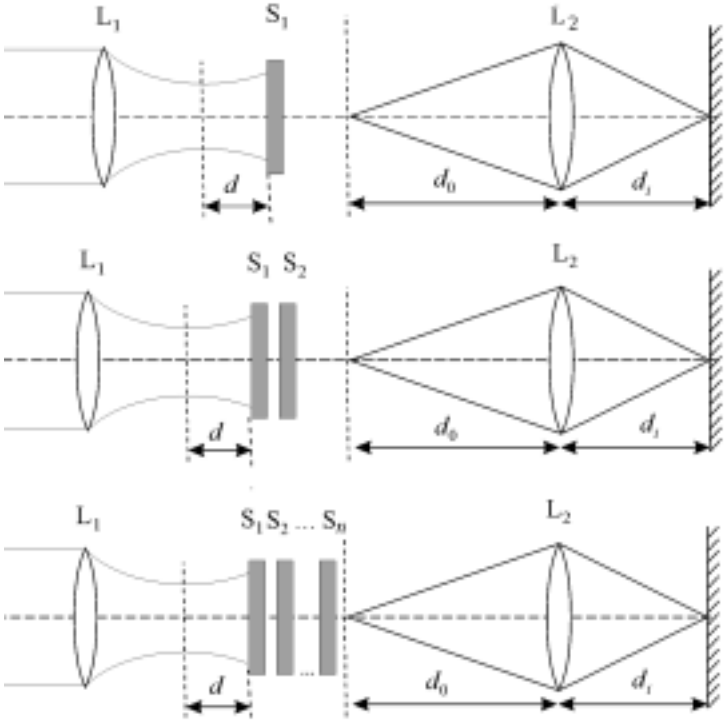

Fig. 2. Illustration of various models used to describe the effects of multiple scattering of the probing laser radiation (L_1, L_2 — lenses; S_1, S_2, S_n — diffusers).

$$\gamma_{\Delta I}(\mathbf{r}, \tau) = \exp\left(-\frac{|\mathbf{r}|^2}{r_s^2}\right)\exp\left[-\frac{(\tau - \tau_d)^2}{\tau_c^2}\right], \tag{3}$$

where $\mathbf{r} = \mathbf{r}_2 - \mathbf{r}_1$, $\tau = t_2 - t_1$ and the delay time t_d depends on $\mathbf{r}$.

Influence of Multiple Scattering on the Speckle-Field Dynamics. The simplest model that can be used to describe the effects of multiple scattering is shown in Fig. 2. It is a set of completely diffusing diffusers (matted plates) moving at different velocities. The statistics of speckle-fields generated by such systems was investigated in [9–13]. In [13], the approximation of a "thin" completely diffusing diffuser and in [9–12] the approximation of a "deep" phase plate were used. The latter is better suited for describing the scattering processes in dense biological media.

For an isolated plate moving at a constant velocity $\mathbf{v}$, the values of τ_c and τ_d are expressed in terms of the parameters of the optical system

$$\tau_c = \frac{1}{|\mathbf{v}|}\left[\frac{\sigma_i}{D^2} + \frac{d_i}{r_s^2}\left(\varepsilon\sigma_i - \frac{1}{d_0}\right)^2\right]^{1/2}, \quad \tau_d = \frac{\tau_c^2 d_i^2}{r_s^2}\left(\varepsilon\sigma_i - \frac{1}{d_0}\right)\mathbf{v}\cdot\mathbf{r}, \tag{4}$$

where d_0 is the distance from the object's plane to the imaging lens; d_i is the distance from the lens to the observation plane; $\varepsilon = 1/d_0 + 1/d_i - 1/r$ and $\sigma_i = 1 + d_0/\rho$. The dynamic speckle size r_s' is related to its statistical size $r_c = \pi\lambda d_i/D$ and the displacement value r_t by the relations

$$r_s' = \frac{r_s^2 + r_t^2}{1 + \sin\theta\, r_t^2/r_s^2}, \quad r_t = \frac{d_i D}{\sigma_i}\left(\varepsilon\sigma_i - \frac{1}{d_0}\right). \tag{5}$$

Equation (4) shows that the dynamic speckle-field correlation time is inversely proportional to the velocity of the phase plate creating this field. Precisely (4) serves as the basis for measuring the rate of the near-surface blood flow by the method of dynamic speckle-photography [14–17].

The simplest model that permits taking into account two different diffusers incorporates two phase plates which in the general case can move at different velocities. In the simplest case, one of the plates can be stationary. In this model, the first stationary plate is an analog of the stationary cutaneous tissue scattering the probing radiation and generating a stationary speckle-field which is scattered by the second moving plate — an analog of the blood flow in the subcutaneous capillaries. In turn, the radiation scattered by the second plate is scattered again by the first plate. Such speckle-fields formed as a result of double or triple scattering is sometimes called the double speckle-field ("speckled speckle") [9]. In the general case, τ_c is expressed in terms of both velocities of the diffuser:

$$\tau_c = \sqrt{a_{11}|\mathbf{v}_1|^2 - 2a_{12}\mathbf{v}_1\mathbf{v}_2 + a_{22}|\mathbf{v}_2|^2}\,, \tag{6}$$

where $\mathbf{v}_1$ and $\mathbf{v}_2$ are the velocities of the phase plates and a_{11}, a_{12}, and a_{22} are constants depending on the optical system configuration [9]. Equation (6) shows that the correlation time depends on the rate of motion of each diffuser and this dependence is complicated. However, it was shown in [9] that in two partial cases simpler dependences exist. For instance, at $d = 0$

$$\frac{1}{\tau_c} = |\mathbf{v}_1 - \mathbf{v}_2| \sqrt{\left(\frac{\beta_1^2 + \beta_2^2}{2}\right)}\,, \tag{7}$$

β_1 and β_2 are effective correlation lengths of the first and second diffusers. When the first diffuser is illuminated by a divergent Gaussian beam in the case of lens-free recording of the speckle-field, the correlation time is determined by the relation

$$\frac{1}{\tau_c} = \left(\frac{2}{\beta_1^2}|\mathbf{v}_1|^2 + \frac{2}{\beta_2^2}|\mathbf{v}_2|^2\right)^{1/2}. \tag{8}$$

For $\beta_1 = \beta_2 = \beta$, Eq. (8) is simplified:

$$\frac{1}{\tau_c} = \frac{2v_a}{\beta}, \tag{9}$$

here $v_a = \sqrt{\dfrac{|\mathbf{v}_1|^2 + |\mathbf{v}_2|^2}{2}}$ is the value of the rms velocity.

There is a possibility of changing dependence (6) by focusing the lens L_2 on different planes in the image space. For instance, when it is focused on the first diffuser at a distance between the plates larger than the spot size in the focus we have

$$\gamma_{\Delta I}(0, \tau) = \exp\left(-\frac{1}{r_0^2}|\mathbf{v}_1|^2\tau^2\right). \tag{10}$$

In focusing on the second diffuser

$$\gamma_{\Delta I}(0, \tau) = \exp\left(-\frac{1}{r_0^2}|\mathbf{v}_2|^2\tau^2\right), \tag{11}$$

and in the case of focusing on the plane lying between the diffusers, we obtain

$$\gamma_{\Delta I}(0, \tau) = \exp\left(-\frac{1}{r_0^2}\left|\frac{\mathbf{v}_1 + \mathbf{v}_2}{2}\right|^2\tau^2\right), \tag{12}$$

where r_0 is the Airy disk for lens L_2 images.

For the illumination by a Gaussian beam by means of the lens L_1 focused on the first diffuser,

$$\gamma_{\Delta I}(0, \tau) = \exp\left(-\frac{1}{\xi_2} |\mathbf{v}_1 - \mathbf{v}_2|^2 \tau^2\right). \quad (13)$$

Figure 2 gives the optical configuration for calculating the space-time correlation function of the speckle-field formed as a result of the processes of multiple scattering by space plates moving in parallel with each other at different velocities. When these plates are illuminated by coherent radiation, the dynamic speckle-field is formed in the image plane of the lens. The direct numerical investigation of the diffraction processes in such a system has shown that the presence of different rates of motion of the phase plates leads to a considerable change in the space-time correlation function of the resulting speckle-field.

Important parameters in investigating the correlation time of the dynamic field are the resolution of the imaging lens and the position of its focal plane when focused on the object. As mentioned above, in the case of two diffusers it is possible to determine the rates of their motion by focusing the imaging lens on them. In so doing, it is essential that the Airy disk of this lens on the object be smaller than the size of the speckles on the second diffuser. Interestingly, such a situation also remains when the number of diffusers is increased. For instance, even for five diffusers moving at different rates the dependence of the correlation time on the velocity of the plate on which the imaging lens is focused remains stronger, although, naturally, the "interfering" action of the other plates gains in strength.

Proceeding to an infinite number of plates, we will characterize the spread in the travel velocities by the dispersion and introduce their mean velocity. Let the velocity distribution be Gaussian; then the standard (rms) deviation of the velocity will characterize its dispersion.

The results of the calculations [10, 11] show that in the case of a large Airy disk of the imaging lens the correlation time of the dynamic speckle-field appears to be practically independent of the mean velocity, while a strong dependence is noted for small sizes of the Airy disk. From this it follows that for high-resolution imaging systems the correlation time of the obtained dynamic speckle-field is largely determined by the absolute values of the diffuser velocities and not by their relative difference. At the same time, when a lens-free configuration of recording obtained speckle-fields is used, the situation is the reverse and the value of the correlation time is largely determined by the dispersion of the diffuser velocities. Naturally, the same situation is observed in the case of using low-resolution imaging systems.

Thus, adjusting the optical dynamic speckle-field recording system, one can determine both parameters characterizing the motions of the diffusers, i.e., their mean velocity and its dispersion. The most difficult case for diagnostics is the situation where the value of the velocity dispersion is comparable to the mean velocity of travel of the diffusers.

Both theoretical and direct experimental studies [9] have shown that equations similar to those discussed for a single diffuser can successively be used for configurations incorporating both two and three diffusers moving at different rates as well. Recent numerical investigations [11] have shown that the value of τ_c for certain optical configurations almost linearly depends on the mean velocity of the scatterer for an infinite number of diffusers as well. This makes it possible to extend the application of the relations for a single diffuser to the case where, in the first approximation, the effects of multiple scattering are taken into account. It should be emphasized that dynamic speckle-fields are more complicated than particle flows in the selected plane in the PIV technique, where such regimes as "boiling" are absent.[1)]

Method of Digital Dynamic Speckle-Photography and Description of the Experimental Procedure. In using the "classical" photographic technique, "instantaneous" recording of speckle-fields is carried out at two different instants of time. Then the negative is developed and the obtained specklegram is subjected to optical analysis in order to determine the averaged displacement of particles in each minor subregion ("subzone") of the negative (specklegram) corresponding to a certain minor region of the flow. As a result, the flow velocity vector in each "subzone," the num-

[1)]An analog of "boiling" in the PIV technique is the departure of particles from the observation plane because of the three-dimensionality of the flow. As for the "boiling" of biospeckles, this phenomenon leads to a decorrelation of speckle-fields. We use the values of this decorrelation and the correlation time τ_c to obtain quantitative information about the near-surface blood-flow intensity in living biological tissues.

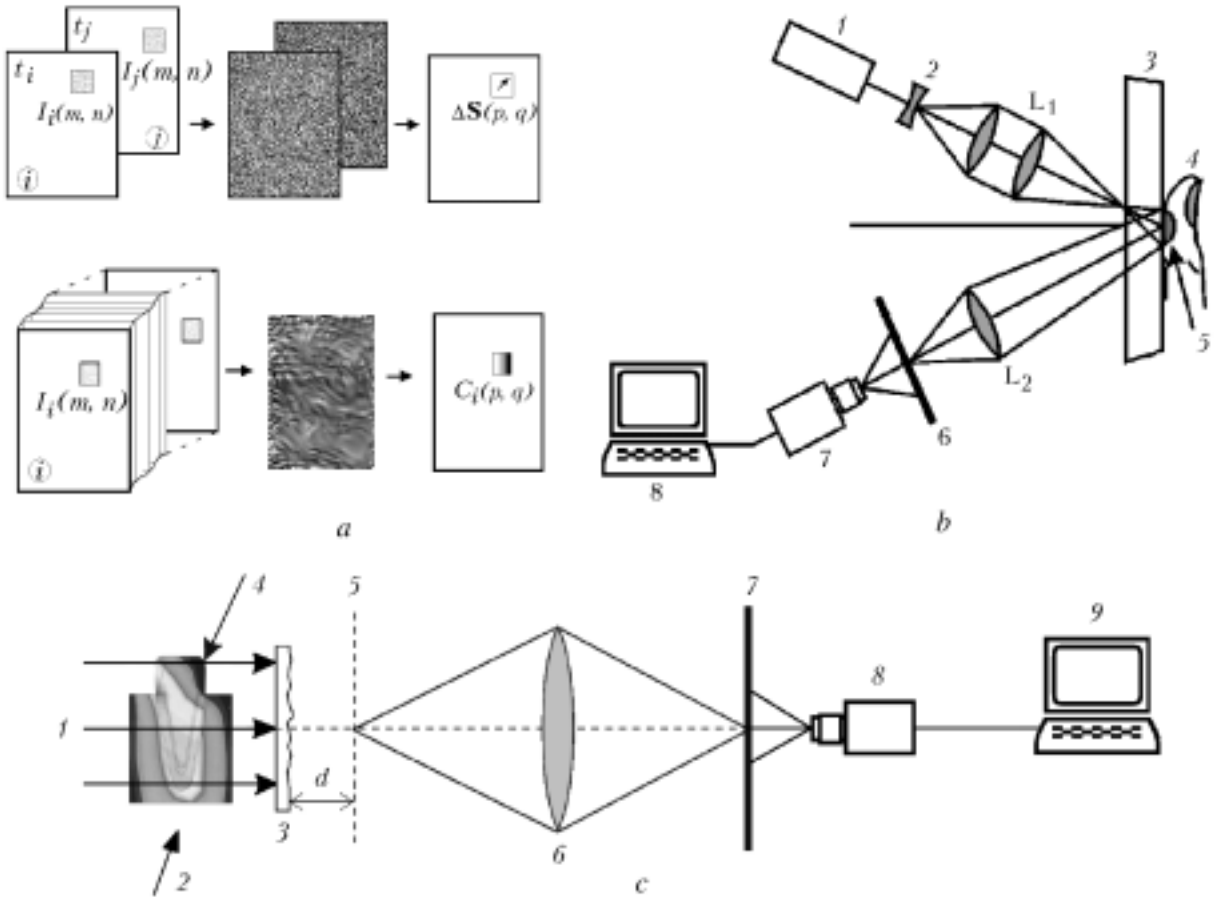

Fig. 3. Block-diagrams: a) digital processing of obtained information (in the upper part — cross-correlation analysis, in the lower part — autocorrelation analysis); b) facilities for investigating soft biological tissues (1 — laser, 2 — collimator, 3 — transparent glass, 4 — biological tissue *in vivo*, 5 — illuminated volume; 6 — recording plane, 7 — CCD-camera, 8 — PC); b) facilities for dynamic speckle-photography of semitransparent objects (1 — probing laser radiation, 2 — semitransparent object being investigated, 3 — matte plate, 4 — load, 5 — focusing plane, 6 — imaging lens, 7 — registration plane, 8 — CCD-camera, 9 — PC).

ber of which can be very large ($\sim 10^{-6}$ or more, see [7]) is determined. Exactly this fact — the possibility of obtaining experimental data bulks with their subsequent statistical processing — has dictated the significant advances in speckle-photography in investigating complex three-dimensional turbulent flows, whose analysis and description are possible only with the use of high-precision statistical methods [5].

An apparent disadvantage of this and analogous photographic systems is the need for photographic processing of negatives, which requires special conditions and time. The situation radically changes when speckle-fields are recorded digitally. In this case, the optical processing of the specklegram can be replaced by its numerical cross-correlation analysis permitting determination of the same parameter — the averaged speckle displacement vector in each selected subzone of the digital specklogram stored in the PC memory. Indeed, let the intensity distribution in the speckle-field recorded by means of a CCD-camera with the number of elementary cells $M \times N$ be described by the function $I_i(m, n)$, where i is the exposure number and $m \in (1, 2, ..., M)$ and $n \in (1, 2, ..., N)$ (see Fig. 3a). Comparing the two images, one can determine their cross-correlation function $R_{ij}(\Delta\mathbf{S}) = \dfrac{\langle I_i(\mathbf{S}) \cdot I_j(\mathbf{S} + \Delta\mathbf{S}) \rangle}{\langle I_i \rangle \langle I_j \rangle}$.

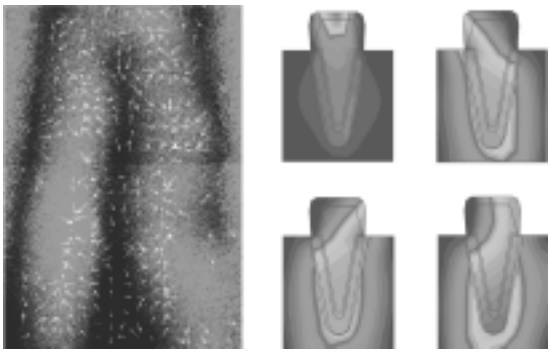

Fig. 4. Digital speckle-photograph of the experimental model cast stump-pin implant-tooth root with a load applied (on the left). Stress-field in the model pin structure–tooth root (on the right).

$$R_{ij}(p, q) = \frac{MN}{(M-p)(N-q)} \left[\frac{\sum_{m=1}^{M-p} \sum_{n=1}^{N-q} I_i(m, n)\, I_j(m+p, n+q)}{\sum_{m=1}^{M} \sum_{n=1}^{N} I_i(m, n)\, I_j(m, n)} \right]. \qquad (14)$$

In the general case, R_{ij} is a function of two vector variables **S** and Δ**S** and time $R_{ij} = R_{ij}$ (**S**, Δ**S**, t). In the so-called homogeneous or quasi-homogeneous fields, this function no longer depends on the coordinate **S** and remains only a function of the displacement Δ**S**. The values of the vector $\Delta\mathbf{S} = \mathbf{i}\cdot p^* + \mathbf{j}\cdot q^*$ determine the speckle displacement vector averaged over the entire specklegram field in the time between exposures i and j. The coordinates (p^* and q^*) definitively characterize the position of the point at which the correlation function acquires its maximum value. This value is equal to unity in the case where the speckle-fields during the first and second exposures are identical and only displaced as a unit to the vector Δ**S**, $R_{ij}^*(p^*, q^*) = 1$. In the case where the speckle-fields, when moving, change in a particular way, $0 < R_{ij}^*(p^*, q^*) < 1$. In analyzing such situations, which correspond to the speckle-photography of biological objects, it is necessary to break up the specklegram being analyzed into small "subzones" in each of which the vectors of averaged displacements of speckle-fields will be found. The values of M and N in relation (14) will correspond to the number of cells in the "subzone." In using "standard" CCD-cameras with $\sim 1000 \times 1000$ cells, the number of "subzones" can amount to $\sim 32 \times 32$, 64×64, and even 128×128. In this case, the number of elementary cells in each "subzone" remains sufficient for statistical averaging in calculating the cross-correlation function. Such calculations on modern PCs can be carried out in the time interval between sequential frames in recording digital images in the TV standard (at a frequency of 25 Hz this interval is 40 msec), which opens up the possibility of constructing systems of real-time diagnostics. In the present paper, a program of "quasi-real-time" processing of images, the calculation and analysis of the correlation function (14) by which requires ~300 msec on a medium-class (Pentium) PC, has been realized. In so doing, the frequency of processed information output onto the monitor is 1–2 Hz, which is enough for direct visualization of relatively low-frequency processes, e.g., smooth spatial and slow temporal changes in the near-surface blood flow *in vivo* [18–23].

The block-diagrams of various systems of digital recording of dynamic speckle-fields used at the A. V. Luikov Heat and Mass Transfer Institute (HMTI) of the NAS of Belarus are shown in Fig. 3a and c). In investigating soft tissues, the dynamic biospeckle-field was generated by the biological tissue being investigated upon its probing *in vivo* by coherent laser radiation via the above-described processes of multiple scattering of light by moving erythrocytes. Hard biological tissues were investigated on specially made semitransparent models. The speckle-field thereby was generated under illumination of the matte plate by laser radiation. As a laser, we used a Melles Griot He–Ne laser of power 10 mV. In both cases, the generated speckle-field was recorded by a JAI Corp. CCD-camera (Japan). The CCD-camera contains 768×494 sensitive cells located on a 6.45×4.84 mm matrix. The exposure time in the case of using this CCD-camera can be varied between 1/6 sec and 10 μsec. The recording frequency is 25 frames per sec-

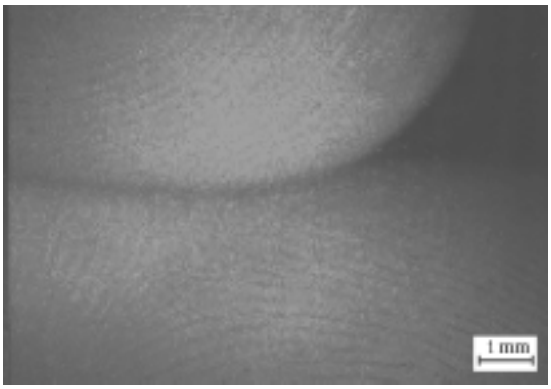

Fig. 5. Biospeckle-field sample recorded by means of a CCD-camera. The size of the investigated field is 2×2 mm^2 and the spatial resolution is 768×494 points.

ond. The signal from the CCD-camera arrives at an A/D converter (digitizer) (16 bits) and the PC graphics card, having its own storage of 2 Mb (megabytes). In so doing, the the computer memory (64 Mb) is also used.

Investigations of soft tissues *in vivo* were conducted on various portions of human biological tissue upon its probing by an extremely low-power laser radiation. As a hard biological tissue model, the system stump-pin implant-tooth root served. A three-dimensional full-sized model of the central incisor of the upper jaw was constructed from an optically sensitive material (polymer). The cast stump-pin implant in the model was made of stainless steel. The pin length was 2/3 of the root length. To imitate elasticity of periodontal fibers, a rubber spacer was placed between the model and the tooth root. The model was fixed in a lock and placed on the bearer frame of the setup.

The load on the pin structure had a concentrated character and was applied in the region of the cutting edge vertically to the central axis of the tooth. The load value was 100 N. The experimental results were processed by a program developed in the Laboratory of Convective and Wave Processes of the HMTI of the NAS of Belarus. Figure 4 shows the digital speckle-photograph of the experimental model cast stump-pin implant-tooth root with an applied load. It depicts the result of the processing of the experimental model's speckle-field. By the position and value of the displacement vectors in this figure one can judge the stressed-strained state in the model. This figure also presents the results of the numerical modeling of the stressed state in the system under consideration. Analyzing the digital speckle-photograph, note that the concentration of maximum stresses is localized in the apical part of the tooth in the region of the pin top as well as in the near-neck region (contact zone of the crown part of the cast stump-pin implant with the tooth model). In the remaining part of the experimental model the distribution of stresses is more uniform. Figure 5 shows a sample of the initial biospeckle-field obtained in probing a biological tissue by He–Ne laser radiation. The results of the direct numerical analysis of fields of such a kind recorded in digital form are given below.

Experimental Studies of the Dynamics of Nonstationary Biospeckle-Fields. The temporal evolution of biospeckle-fields can be analyzed using relation (14) by comparing the values calculated for various instants of time. The employment of the so-called structural function widely used in describing the turbulence

$$D_{I_{1-2}}(p, q) = \frac{NM}{(N-p)(M-q)} \left[\frac{\sum_{n=1}^{N-p} \sum_{m=1}^{M-q} \left(I_1(n, m)\, I_2(n+p, m+q)\right)^2}{\sum_{n=1}^{N} \sum_{m=1}^{M} I_1(n, m)\, I_2(n, m)} \right] \tag{15}$$

is somewhat more effective. An analogous function referred to as the "decorrelation parameter" was also used in [24, 25] in investigating biospeckle-fields generated by living plants. Figure 6 gives the data on such a function for various samples obtained on different experimental facilities. The left-hand part of the figure shows the data obtained with the aid of a "standard" CCD-camera operating in the TV standard. The changes in the structural function are shown on this plot depending on the frame number (the interval between frames is 40 msec). As is seen from these data, for

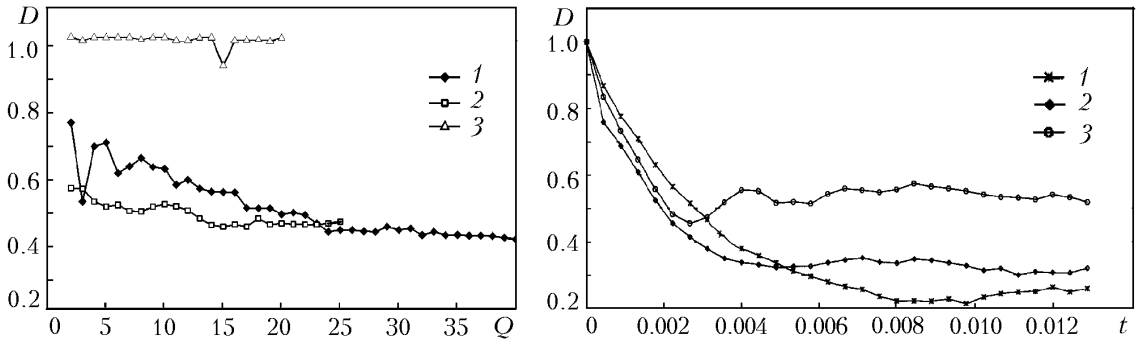

Fig. 6. Time change in the structural function D for various biological tissues; on the left: 1 — blood flow *in vivo*; 2 — apple pulp; 3 — concrete (for control) (on the horizontal axis — number of frames); on the right: 1–3 — portions of human skin (on the hand) with different blood-flow intensities. t, sec.

both biological tissues the structural function experiences a sharp decrease in the first 40 msec followed by slow changes during 10–20 frames. The constant structural function of the stationary speckle field is shown here for control. The right-hand part of the figure shows the data obtained at Poitiers University (Université de Poitiers, France) by a unique high-speed CCD-camera with a frequency of taking up to 2000 frames per second [26]. They clearly show that in the dynamic field generated by the subcutaneous blood flow very high frequencies of up to 1–2 kHz are present. This places special requirements on the recording devices for total reflection of the high-frequency part of the spectrum of the dynamic speckle-field, especially in real-time.

Such high-frequency processes can be visualized in real or quasi-real time in the scheme of the so-called single-exposure photography [27]. In this case, each speckle-field recorded in the CCD-camera for a longer time comparable to the characteristic time of the fast process under investigation is analyzed (see Fig. 3b). At such a recording the image blurs and its contrast decreases. In this connection, the contrast value of the time-integrated speckle-field can serve as a characteristic of the averaged displacement of speckles in the exposure time. In Professor Briers' works devoted to the investigation of blood flow by the contrast of the speckle-fields arising under light scattering by moving erythrocytes, it is shown that the contrast value is inversely proportional to the rate of their motion [15–17].

The speckle-field contrast is calculated by the relation

$$C_i = \frac{\sigma_{I_i}}{\langle I_i \rangle} = \frac{\sqrt{\langle I_i \rangle^2 - \langle I_i^2 \rangle}}{\langle I_i \rangle} = \sqrt{\left[\frac{1}{MN} \sum_{m=1}^{M} \sum_{n=1}^{N} I_i \right]^2 - \frac{1}{MN} \sum_{m=1}^{M} \sum_{n=1}^{N} I_i^2} \Big/ \left(\frac{1}{MN} \sum_{m=1}^{M} \sum_{n=1}^{N} I_i \right). \qquad (16)$$

Here M and N, as in (14), determine the number of elementary cells in the CCD-camera in analyzing motions uniform throughout the field or the number of cells in the "subzone" in analyzing complex (quasi-homogeneous) fields. The speckle-field contrast is a scalar quantity, but in the case where the specklegram is broken up into subzones, it is a function of two coordinates: $C_i = C_i(p, q)$. It is no longer necessary to calculate the maximum of this function and the contrast value can be associated with the absolute value of the velocity at the investigated point $\langle \mathbf{v}(p, q, t) \rangle$. The value of this contrast as well as the values of the near-surface blood-flow intensity obtained by it in the form of a time sequence of isolines obtained in quasi-real time are given in Fig. 7.

In the general case, the velocity direction is not determined by means of direct autocorrelation analysis. This can only be done by means of various additional techniques [7]. Note that the autocorrelation analysis by relation (16) is much simpler than the cross-correlation one, which makes it possible to increase the frequency of real- or quasi-real-time information output onto the monitors. This frequency can easily be brought up to 25 Hz even with the use of a medium-scale PC. However, the chief advantage of the single-exposure technique is the possibility of greatly increasing the rate of change in the process under investigation. This rate in the given scheme is associated not with the time interval between sequential frames but with the recording time of each image, which in standard CCD-cameras

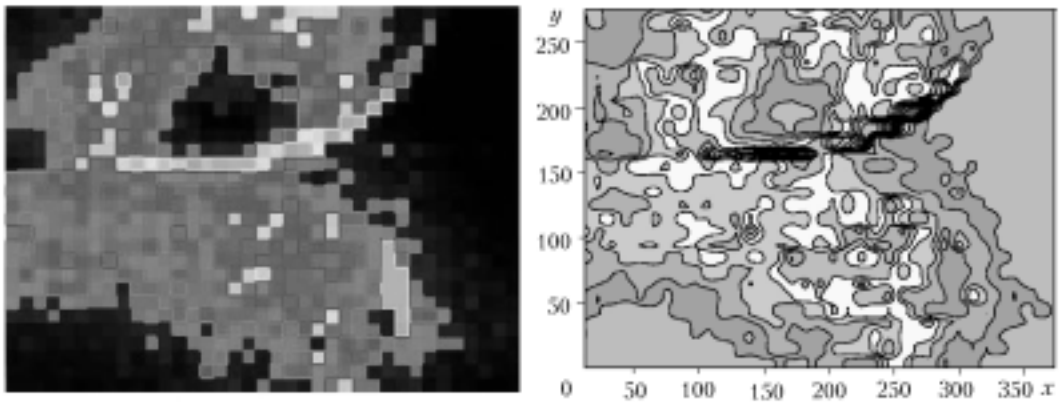

Fig. 7. Isolines of the speckle-field contrast (on the left) and the value of the near-surface blood flow (on the right) in conventional units at different instants of time.

can be varied from 10 to 40 msec. Exactly this fact permits investigating, with the use of the single-exposure technique, processes with characteristic frequencies of up to 100 kHz (and higher by using special shutters).

In the regime of quasi-real-time recording, processing of obtained images was carried out by two different techniques. In using cross-correlation analysis, function (14) (its amplitude and maximum coordinates) are calculated by two sequential frames. The results of the calculation are output onto the monitor, and the PC begins to process the next frames.

In the autocorrelated analysis, the speckle-field contrast in each subzone is calculated. The calculation time is ~100 msec, which practically provides quasi-real-time calculation with a frequency of ~ 10 Hz.

CONCLUSIONS

In the present paper, we have shown that in principle it is possible to investigate ultrafast processes by means of digital speckle-photography in quasi-real-time. It has been shown that multiple-scattering processes make a significant contribution to the formation of dynamic biospeckle-fields in which frequencies of up to 1–2 kHz have been registered. Simple engineering relations describing the dynamics of these fields are given. Examples of investigating both soft and hard biological tissues on the basis of statistical analysis of the dynamics of change in biospeckle-fields registered in PC storage in digital form with the aid of high-resolution CCD-matrices are given.

The authors express deep gratitude to the international organization INTAS and the government of the Republic of Belarus for financial support under joint grant INTAS-BELA 97-0082 and INTAS grant 00-0135 as well as to the Belarus Basic Research Foundation for financial support of the investigations under grant T02R-043.

NOTATION

a_{11}, a_{12}, a_{22}, coefficients; C_i, speckle-field contrast; D, lens diameter, m; D_I, structural function; d, d_0, d_i, distances, m; I, laser radiation power density, W/m^2; (m, n), cell number of the CCD-matrix; M, N, CCD-matrix size; (p, q), current coordinates of the cross-correlation function of intensity R_I; (p^*, q^*), coordinates of the function R_I maximum; Q, number of frames (see Fig. 6); r_s, statistical size of the speckle, m; r_s', dynamic size of the speckle, m; r_t, displacement value, m; r_0, radius of the Airy disk of the imaging lens, m; $\Delta\mathbf{S}$, displacement vector, m; t, time, sec; t_i and t_j, time of the ith and jth exposure; $\mathbf{v}$, velocity, m/sec; v_a, rms velocity, m/sec; x, y, sizes (see Fig. 7), pixels; z, $\mathbf{r}$, spatial coordinates, m; z_0, characteristic scale (see relation (2)), m; β_i, effective correlation length of the ith diffuser, m; $\gamma_{\Delta I}$, cross-correlation coefficient; ε, defocusing parameter; θ, angle between vectors $\mathbf{r}$ and $\mathbf{v}$, rad; λ, laser-radiation wavelength, m; ρ, wavefront curvature, m; σ_i, parameter; σ_{I_i}, rms deviation of laser radiation at the ith point, W/cm^2; τ, time interval, sec; τ_c, correlation time, sec; τ_d, delay time, sec; ω, current diameter of the laser spot, m; ω_0, laser spot diameter in the neck (in focus), m. Subscripts: a, average; c, correlation; d, delay; s, speckle; t, displacement; $\langle ... \rangle$, mean value of a quantity.

REFERENCES

1. J. D. Briers and A. F. Fercher, *Invest. Ophth. Vis. Sci.*, **22**, 255–259 (1982).
2. Y. Aizu and T. Asakura, *Proc. of SPIE Conf. on Time Resolved Spectroscopy and Imaging of Tissues*, Bellingham, **1431**, 239–250 (1991).
3. N. Konishi and H. Fujii, *Opt. Eng.*, **34**, 753–757 (1995).
4. N. Fomin, C. Fuentes, J.-B. Saulnier, and J.-L. Tuhault, *Laser Phys.*, **11**, No. 4, 525–529 (2001).
5. N. Fomin, *Speckle Photography for Fluid Mechanics Measurements*, Berlin (1998).
6. N. B. Bazylev, S. M. Vlasenko, E. I. Lavinskaya, and N. A. Fomin, *Dokl. Nats. Akad. Nauk Belarusi*, **45**, No. 5, 55–59 (2001).
7. J. Kompenhans, M. Raffel, and C. E. Willert, *Particle Image Velocimetry: A Practical Guide*, Berlin (1998).
8. T. Asakura and N. Takai, *J. Appl. Phys.*, **25**, 179–194 (1981).
9. T. Okamoto and T. Asakura, *J. Mod. Optics*, **37**, 389–408 (1990).
10. T. Okamoto and T. Asakura, *Waves in Random Media*, **2**, 49–65 (1992).
11. T. Okamoto and T. Asakura, in: E. Wolf (ed.), *Progress in Optics*, Vol. XXXIV, Amsterdam (1995), pp. 183–248.
12. T. Yamaguchi, in: R. S. Sirohi (ed.), *Speckle Metrology*, Marcel Dekker, New York (1993), pp. 27–42.
13. B. J. Uschinski, *Wave Propagation in Random Media* (*Scintillation*), Bellingham (1993), pp. 346–357.
14. J. D. Briers, *Optik*, **63**, No. 3, 265–276 (1983).
15. J. D. Briers, *Opt. Eng.*, **32**, 277–283 (1993).
16. J. D. Briers, *SPIE Proc.*, Bellingham–Washington, **2083**, 238–249 (1994).
17. J. D. Briers, in: *Proc. of SPIE Conf. "CIS Selected Papers: Coherent-Domain Methods in Biomedical Optics,"* Bellingham, **2732** (1996), pp. 2–15.
18. N. Fomin, C. Fuentes, J.-B. Saulnier, and J.-L. Tuhault, in: J.-B. Saulnier, D. Lemonnier, and J.-P. Bardon (eds.), *Proc. of Microscale Heat Transfer EUROTHERM Seminar*, No. 57, Futuroscope, France, 8–10 July, 1998, pp. 233–240.
19. N. Fomin, C. Fuentes, J.-B. Saulnier, and J.-L. Tuhault, in: *Proc. of the 9th Int. Symp. on Flow Visualization*, Edinburgh (2000), pp. 89.1–89.8.
20. S. P. Rubnikovich, N. A. Fomin, and N. B. Bazylev, *Sovr. Stomatol.*, No. 2, 44–46 (2001).
21. N. A. Fomin, S. P. Rubnikovich, and N. B. Bazylev, *Sovr. Stomatol.*, No. 3, 50–52 (2001).
22. N. Bazylev, N. Fomin, T. Hirano, E. Lavinskaya, T. Mizukaki, A. Nakagawa, S. Rubnikovich, and K. Takayama, in: *CD-ROM Proc. of the 10th Int. Symp. on Flow Visualization*, Kyoto, Japan (2002), Paper F0042.
23. N. Bazylev, N. Fomin, C. Fuentes, C. Hirano, E. Lavinskaya, S. Martemianov, T. Mizukaki, A. Nakagawa, S. Rubnikovich, J.-B. Saulnier, K. Takayama, and J.-L. Tuhault, in: *Proc. of 11th Int. Laser Physics Workshop*, 2002 (LPHYS'02), Bratislava, Slovakia (2002), p. 116.
24. N. B. Bazylev, N. A. Fomin, E. I. Lavinskaya, and S. P. Rubnikovich, in: *Proc. of 13th Conf. of Eur. Soc. of Biomechanics*, Wroclaw, Poland, 1–4 September 2002, in *Acta of Bioengineering and Biomechanics*, **4**, Suppl. 1, (2002), pp. 510–511.
25. A. Oulamara, G. Tribillon, and J. Duvernoy, *J. Modern Optics*, **36**, No. 2, 165–179 (1989).
26. C. Fuentes, J.-L. Tuhault, N. Fomin, et J.-B. Saulnier, in: *Journée SFT "Microconvection et systémes miniaturisés,"* Lyon, France (2000), pp. 1–16.
27. A. M. Fercher and J. D. Briers, *Opt. Commun.*, **37**, 326–330 (1981).